




Electrochemical performance evaluation of a newly developed ZnS–SnO₂ composite in an aqueous electrolyte

Kinza Rafique^{1,2}, Muhammad Zia Ullah Shah^{2,3}, A. Shah^{2,*}, Muhammad Sana Ullah Shah^{2,3}, Hongying Hou³, Muhammad Sajjad^{4,*} , Muhammad Arif^{2,3}, Syed Awais Ahmad^{2,3}, and Najmul Hassan^{1,*}

¹ Department of Physics, Hazara University, Mansehra 21300, Pakistan

² National Institute of Lasers and Optronics College, Pakistan Institute of Engineering and Applied Sciences, Nilore, Islamabad 45650, Pakistan

³ Faculty of Materials Science and Engineering, Kunming University of Science and Technology, Kunming 650093, People's Republic of China

⁴ College of Chemistry and Materials Science, Zhejiang Normal University, Jinhua 321004, People's Republic of China

Received: 25 March 2023

Accepted: 7 August 2023

Published online:
26 August 2023

© The Author(s), under exclusive licence to Springer Science+Business Media, LLC, part of Springer Nature, 2023

ABSTRACT

We reported the sol–gel synthesis for preparing ZnS and SnO₂ products and their composite material, for the first time for application as an electrode for a hybrid supercapacitor to attain an optimized energy storage performance. The structural feature reveals that the high phase purity and crystallinity with tetragonal SnO₂, and in the cubic crystal structure of ZnS has been successfully verified from XRD analysis. A snow-like morphology of SnO₂ and irregular nanoparticles in shape with a honeycomb-like appearance of ZnS and their combination that is detected in the ZnS–SnO₂ composite without any residues was noticed on the surface of the samples, which was confirmed from the FESEM study. The electrochemical properties demonstrated that the ZnS–SnO₂ composite manifests more awesome performance than its bulk materials, e.g., 466 F/g of capacitance, good rate performance, and reversibility with good charge transport properties. These striking results motivated us to fabricate a hybrid supercapacitor for practical aspects of the as-prepared electrode material. To do so, a ZnS–SnO₂||AC/KOH hybrid supercapacitor was fabricated, which delivers a good stability of 85.7% (7000 cycles) and supreme power delivery of 4238.4 W/kg. A great specific energy of 36.12 Wh/kg after adding an optimum voltage of 1.7 V. These outstanding outcomes manifest the promising route to prepare another metal oxide/hydroxide for electrochemical energy conversion and storage devices.

Address correspondence to E-mail: attashah168@gmail.com; sajjadfisica@gmail.com; najamalhassan@yahoo.com

1 Introduction

Energy storage has grown to be a significant difficulty for the world's power networks in response to the issue of global warming. This highlights the critical need for efficient and secure energy storage solutions alongside the rise of renewable, clean energy sources [1–6]. Compared to secondary batteries and conventional capacitors, the Supercapacitor (SCs) has many benefits, including high-power density, fast charge, discharge process, excellent cycle stability, quick dynamic response, longer life than ordinary batteries, low cost, environmental friendliness, and safety. Given the SC's benefits, this has led to great concern among researchers. The electrode materials have a major impact on the capacitance of SCs [7–12]. Although SCs have a high-power density, it falls short compared to secondary batteries (such as lithium batteries, sodium-ion batteries, etc.) in terms of energy density. Fabricating SCs with excellent performance requires electrodes with active materials. It is possible to classify active materials into two broad categories, delineated by the techniques by which electrons are stored: Active carbon (AC) carbon nanotubes (CNT) and graphene or doped graphene [13–15] are all examples of the classic kind of electrical double-layered capacitors (EDLCs), which store energy by building up charges in the electrical double layer close to the electrode/electrolyte interface [16–19]. Due to their high-power density and outstanding cyclability, carbon-based materials have been widely used as acceptable electrodes in commercial SCs; nevertheless, their low energy density and capacitance mean they fall short of the needs of modern electronics in other respects [20–23]. There is a high degree of stability throughout the charge/discharge (CD) operation, although their specific capacitance is low. NiO, MnO₂ [24, 25], NiCoO₄ [26], NiCoS [27, 28], and metal-organic frameworks (MOFs) [29] are all examples of electrochemical capacitors that store energy by a Faradaic redox reaction at the electrode surface. SnO₂'s high theoretical capacity (1378 mAh/g), high electrochemical activity, cheap cost, non-toxicity, and outstanding thermal and chemical stability [30, 31] piqued the interest of researchers. Hydrothermal, microwave, solvothermal, and co-precipitation are only a few methods that may be used to create SnO₂ nanostructures. SnO₂@C composite hollow spheres were constructed that yield a capacitance of 25.88 F/g in KOH electrolyte at the concentration of 1 M when utilized as an electrolyte [32]. At a current density of

100 mA/g, the SnO₂@C nanomaterial has an initial discharge and charge capacity of 2589 and 1029 mAh/g, respectively [33]. Zn, Ag-doped SnO₂ nanoparticles made by B. Saravanakumar et al. [34] achieved a specific capacitance of 308.2 F/g at a current density of 0.5 A/g. These electroactive materials have a high theoretical capacitance while lacking mechanical properties and electrical conductivity. Metal sulfides are a new potential family of active materials for energy storage [35–37]. Due to their excellent redox reversibility, comparatively high capacitance, and higher rate capability in SCs. Sulfide atoms can be in two or more valence states [38, 39]. Zinc sulfides (ZnS), one of many transition metal sulfides, have been discovered to be a promising electrode material for SCs. The solvothermal synthesis of NiS₂/ZnS hollow nanospheres and the fabrication of SCs with an energy density of 28.0 Wh/kg at a power density of 478.9 W/kg have been reported [40]. At a scanning rate of 5 mV/s, the ZnS-decorated graphene electrode (ZnS/G-60) displays a maximum specific capacitance of 197.1 F/g [41]. For high-performance flexible all-solid-state SCs, Luo et al. presented an ultrathin ZnS nanosheet/carbon nanotube hybrid electrode with a high specific capacitance of 347.3 F/g [42].

We produced ZnS, SnO₂ NPs, and their nanocomposites utilizing a chemical and hydrothermal technique for excellent ASC performance based on the factors above. The ZnS–SnO₂ composite electrode exhibits an ultrahigh reversible specific capacitance of 466 F/g, outstanding rate capability, and exceptionally excellent cycling stability due to the synergistic effect of our synthesized composite, which significantly improved the capacitance as electrode materials for supercapacitor.

2 Experimental

2.1 Chemicals and reagents

All the solutions were prepared using deionized water (DI). The chemicals used in this study were tin (II) chloride dehydrate, SnCl₂·2H₂O Panreac 97%, and ammonia solution (NH₃ 33%) Na₂S × H₂O and zinc acetate dehydrate [(CH₃COO)₂Zn·2H₂O] were purchased from Panreac, Applichem, Reagents Duksan, and Sigma Aldrich. All reagents were used as received without any further purification.

2.2 Synthesis of SnO₂ nanoparticles

SnO₂ nanoparticles were prepared by the sol-gel method. Generally, 0.85 g SnCl₂·2H₂O was added to 50 ml deionized water and stirred for 20 min. Ammonia solution was then dropwise added until the pH value reached 9 while stirring the solution for 20 min increasing temperature slowly from 30 to 90 °C. The solution was dried in an oven at 90 °C for 2 h. The resulting gel was then washed with ethanol. The obtained powder was grounded and annealed in a muffle furnace at 500 °C for 4 h with a step size of 1 °C rise/min [1].

2.3 Synthesis of ZnS nanoparticles

ZnS nanoparticles were prepared by wet chemical synthesis. A sodium sulfide of 1.5 g was added to 10 ml of DI water. Similarly, zinc acetate dehydrates of 2.1 g were dissolved in 10 ml of DI water separately, mixed in both solutions, and stirred for five hours at room temperature. The nanoparticles were collected by centrifugation for 30 min. The precipitate was then filtered and dried in a laboratory oven at 110 °C for 2 h. After drying, nanoparticles were ground to obtain a fine powder for characterization.

2.4 Synthesis of ZnS–SnO₂ nanocomposites

The synthesis of nanocomposite samples with various ZnS and SnO₂ weight% ratios using a simple wet chemical procedure. ZnS (0.5 g) and SnO₂ (0.5 g) were added to 40 mL of methanol, which was then sonicated for 30 min and stirred for 30 min. The finished product was dried in a lab oven at 60 °C. The prepared SnO₂–ZnS powder was annealed for 3 h at 800 °C.

2.5 Characterization

X-ray diffraction was used to investigate the structural properties of manufactured samples (model: XRD, ARL EQUINOX 3000, thermo scientific made). The crystallite size is calculated using the Scherrer formula. Cu–K α sources with a wavelength of 0.154068 nm are used in the apparatus. Raman spectroscopy investigated the materials' vibration modes (model, Dong-woo Optron Co Ltd). The microstructure of prepared samples was investigated using

field emission scanning electron microscopy (TESCAN FESEM, model: MAIA-3). The Octane Elite detector on the device is used to analyze the elemental composition of the samples.

2.6 Preparation of working electrode and electrochemical measurements

All measurements were performed at room temperature. A Grammarly-300 workstation was utilized for whole electrochemical measurements, in which KOH was employed as the electrolyte. A working electrode (ZnS–SnO₂ composite) was made following steps. (i) A molar ratio of 85:10:5 was taken, in which 85% is the composite material, 10 and 5% are the carbon black and binder, respectively. (ii) These three powders were mixed in an NMP solution to form a slurry with appropriate homogeneity. (iii) The obtained slurry was then coated on Ni foam (current collector). It was kept in a vacuum oven overnight for drying. (iv) After ambient temperature drying, the potential electrode was used for three- and two-electrode testing.

The asymmetric supercapacitors (ASCs) were assembled in a sandwich-type configuration using a ZnS–SnO₂ cathode, activated carbon as an anode in a 3 M KOH electrolyte. All measurements were taken after 24 h to get better adhesion of the electrodes. CV, GCD, and durability were further tested to explore the performance for practical applications.

3 Results and discussion

The proper product formation is confirmed via XRD and Raman analysis, as shown in Fig. 1. The XRD pattern of pure SnO₂ shows peaks at 2θ equal to 26.7°, 33.9°, 38.1°, 51.9°, 54.8°, 57.9°, 61.9°, 64.8°, 65.9°, 71.3°, 78.7°, 81.1°, 83.7°, 87.2°, 89.8°, 90.8°, 93.4°, and 95.9° corresponding to the (110), (101), (200), (211), (220), (002), (310), (112), (301), (202), (321), (400), (222), (330), (312), (411), (420), and (103) planes, respectively (Fig. 1a), which matches with the tetragonal rutile structure of SnO₂ with the standard JCPDS Card no. (01-071-0652). Specifically, the oxygen anions form distorted octahedral arrangements with the metal cations in rutile tetragonal structure configurations. Moreover, the metal cations occupied the interstitial sites, the oxygen atoms were aligned in a closed-packed lattice, and the obtained structural features containing the alternative oxygen and metal cations were arranged as at the

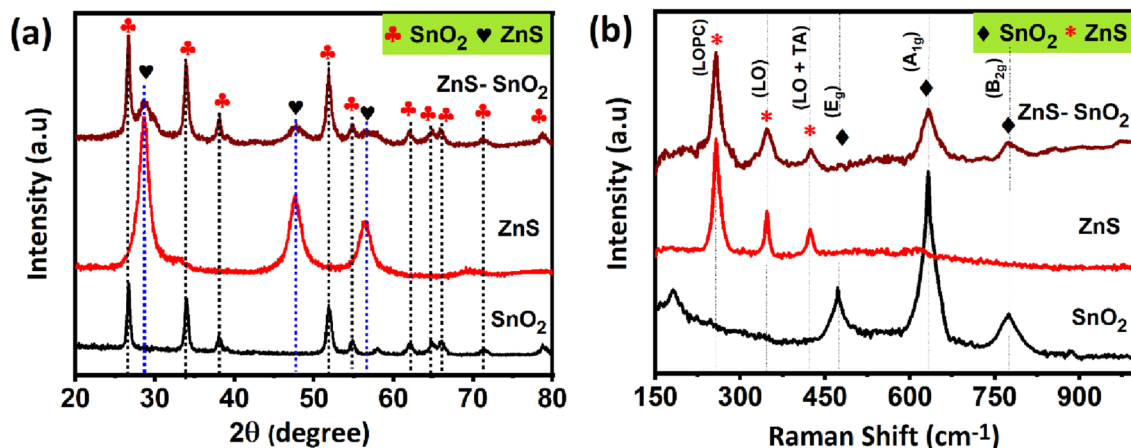


Fig. 1 **a** XRD, **b** Raman shift of the samples ZnS, SnO₂, and ZnS–SnO₂ composite

c-axis unit cell. The specialty of tetragonal rutile symmetry brings some fascinating optical and electronic properties coupled with great stability and symmetry, which is promising for various applications, such as; solar cells, energy storage, and catalysis. Similarly, the three diffraction peaks at the 2θ value are 28.91, 48.06, and 57.28. These peaks can be the reflection from the (111), (220), and (311) planes of the cubic phase of the ZnS. The obtained peak positions correspond to zinc blended-type patterns for all the samples. The XRD pattern matches the standard cubic ZnS (JCPDS Card No. (00-005-0566)). No other impurity phases were observed.

Raman spectra of the ZnS honeycomb morphology range of 100–400 cm^{-1} are shown in Fig. 2b. Raman active modes corresponding to the cubic ZnS in bulk and nanoparticles form are well reported in the literature [43]. The TO and LO zone-center phonons from bulk cubic ZnS were observed near 271 and 352 cm^{-1} , respectively [44]. In the present case, the new ZnS honeycomb shows peaks corresponding to the TO and LO mode at 257 and 348 cm^{-1} and 423 cm^{-1} , respectively. The SnO₂ showed peaks at 478 cm^{-1} , 631 cm^{-1} , and 774 cm^{-1} corresponding to the Raman active modes with E_g , A_{1g} , and B_{2g} in which the latter two are due to the vibrations of Sn–O, and the E_g is related to oxygen vibration [45, 46]. The ZnS–SnO₂ composite displayed the combined appearance of ZnO and SnO₂, revealing the composite's appropriate preparation, which coincides with the XRD results.

The samples' morphology is vital in the performance of supercapacitor electrodes, which can be investigated and analyzed via FESEM analysis.

Figure 2 indicates the FESEM images of the ZnS, SnO₂, and ZnS–SnO₂ composite. The ZnS reveals irregular clusters of nanoparticles with aggregation, as shown in low and high-magnification pictures in Fig. 2a, a1. Moreover, the surface view of the ZnS irregular nanoparticles resembles a honeycomb-like surface architecture, which seems promising for ion storage during the electrochemical process. Also, the SnO₂ showed snow-like morphology that contained thin flakes, as shown in Fig. 2b, b1. Besides, the ZnS–SnO₂ composite morphology was further investigated, which reveals the presence of ZnO irregular nanoparticles and SnO₂ snow-like appearance in the composite, as presented in Fig. 2c. The magnified view of the composite morphology noticed both pure nanomaterials with rough surface appearance, as illustrated in Fig. 2c1. Thus, we expected this type of morphology to be effective for better electrochemical properties, which can be discussed later below.

The EDX analysis explored the formation and composition analysis of the formed nanomaterials and their combination, as depicted in Fig. 3. Based on the EDX studies, the ZnS spectrum reflected only Zn and S peaks. In contrast, Sn and oxygen peaks are detected in the SnO₂ range, as demonstrated in Fig. 3a, b. Meanwhile, a combined appearance of ZnO and SnO₂ in the composite spectrum was seen, as displayed in Fig. 3c. Their corresponding peaks are well observed, indicating the high purity of all samples prepared via the sol–gel method. Thus, the EDX analysis confirms the phase purity of the products, which is consistent with the FESEM and XRD results.

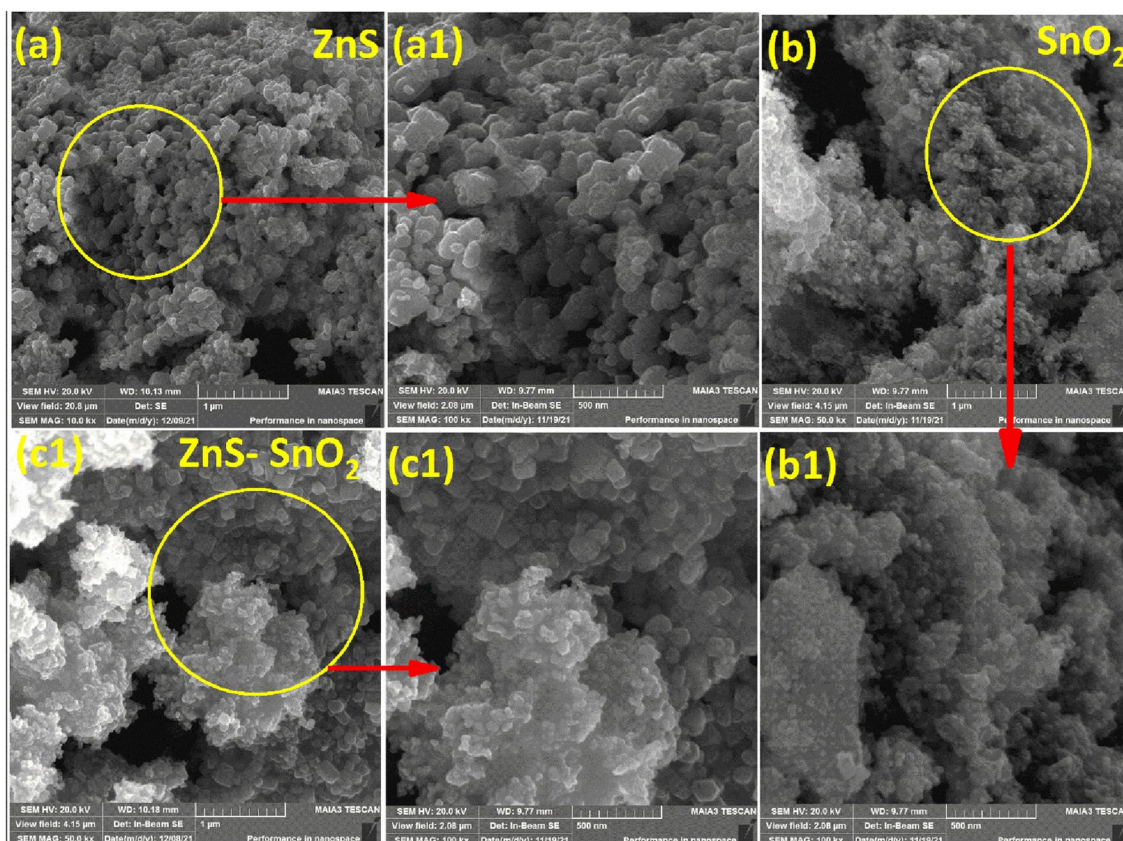


Fig. 2 FESEM images of the sample **a**, **a1** ZnS, **b**, **b1** SnO₂, **c**, **c1** ZnS–SnO₂ composite

The capacitive signature and electrochemical properties of the prepared electrodes ZnS, SnO₂, ZnS–SnO₂ composite can be firstly verified in three-electrode mode using various electrochemical techniques, such as cyclic voltammetry (CV), discharge/charge measurements, and impedance spectroscopy. ZnS, SnO₂, and ZnS–SnO₂ composite electrodes are tested between 0.0 and 0.6 V utilizing an aqueous solution of KOH with 3 millimolar concentration as an electrolyte. The corresponding outcomes from the three-electrode assembly are given in Fig. 4. The comparative voltammogram of the ZnS, SnO₂, and ZnS–SnO₂ composite electrodes is given in Fig. 4a, which revealed that the ZnS–SnO₂ composite electrode encloses the high current response and enclosed loop area, signifying the largest capacitance [47, 48]. Moreover, all electrodes show redox peaks, specifying a typical pseudocapacitive behavior, which can be further verified at varying scans, as demonstrated in Fig. 4b–d. The ZnS electrode followed a similar trend, e.g., shifting of redox peaks towards more negative and positive potential directions due to the high resistance and polarization effect

[49, 50] (see Fig. 4b). Similarly, the SnO₂ and ZnS–SnO₂ composite electrodes also obey the same trend with varying sweep rates, as displayed in Fig. 4c, d. The ZnS–SnO₂ composite electrode enclosed a bigger loop area and response current than ZnS and SnO₂ electrodes, leading to the highest capacitance at similar conditions, which is discussed in Fig. 4a at the start of this section. Additionally, all electrodes sustain the same voltammogram shape from low to higher scans without any distortion noticed, indicating great reversibility and rate capability [39, 51, 52]. The capacitance of the electrodes can be comprehensively calculated from the discharge/charge analysis in the next section.

The energy storage performance can be well achieved using the chronopotentiometry technique with varying current rates for the ZnS, SnO₂, and ZnS–SnO₂ composite electrodes in an aqueous medium in three-electrode configurations with the potential frame ranging from 0.0 to 0.6 V at identical condition, as illustrated in Fig. 5. As shown in Fig. 5a, the comparison of the ZnS, SnO₂, and ZnS–SnO₂ composite electrode has been made in which the

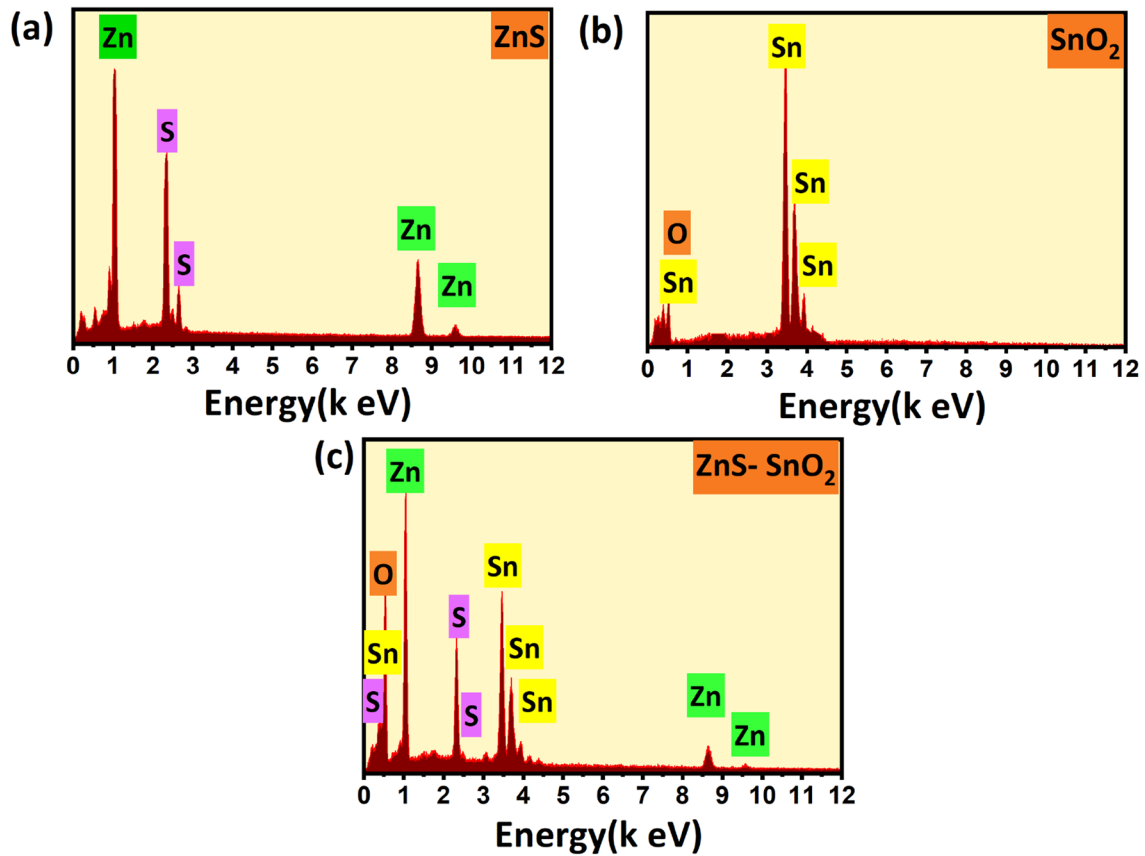


Fig. 3 EDX spectrum of the sample **a** ZnS, **b** SnO₂, **c** ZnS-SnO₂ composite

Fig. 4 Electrochemical performance characteristics of all electrodes, **a** CV voltammogram performance comparison of all electrodes at fixed scan rate, **b–d** CV analysis of the ZnS, SnO₂, and ZnS-SnO₂ composite electrodes at identical conditions

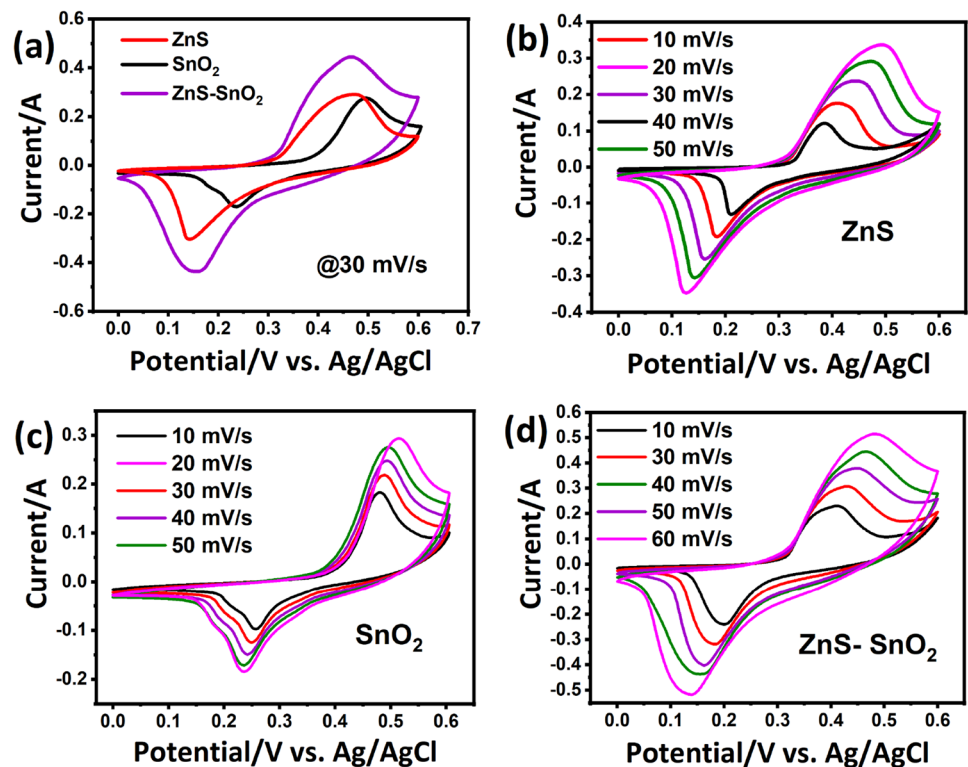
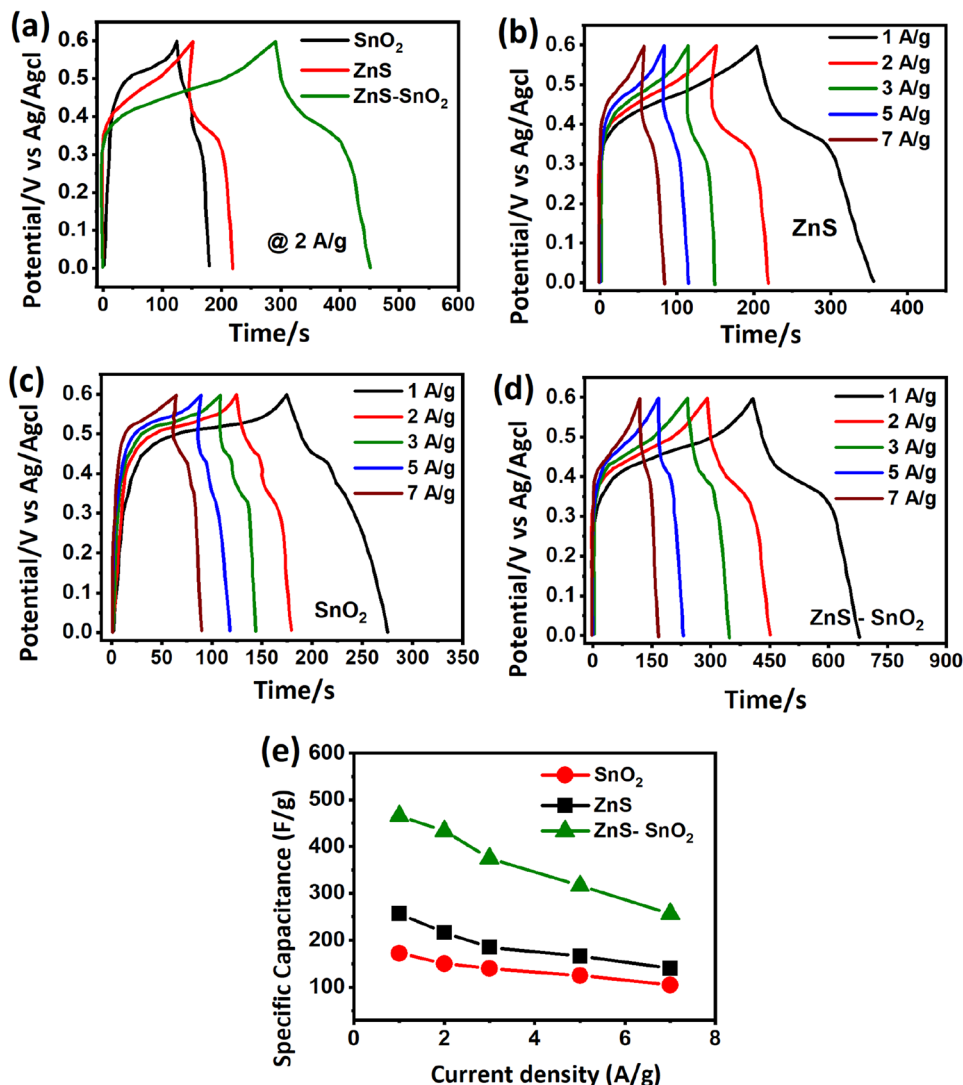


Fig. 5 Chronopotentiometry analysis of all electrodes, **a** discharge/charge characteristics of comparison of all electrodes at the fixed current rate, **b–d** discharge/charge characteristic of the ZnS, SnO₂, and ZnS–SnO₂ composite electrodes at similar conditions, **e** current vs. capacitance graph



ZnS–SnO₂ composite electrode run the race, meaning that the highest discharge time is disclosed than former electrodes. This leads to the largest capacitance of the ZnS–SnO₂ composite electrode (466 F/g than ZnS and SnO₂). The detailed discharge/charge graph of the ZnS, SnO₂, and ZnS–SnO₂ composite electrodes is provided in Fig. 5b–d at several current rates ranging from 1 to 7 A/g. All electrodes showed a typical pseudocapacitive behavior with clear voltage plateaus, consistent with the CV results. Based on Eq. (1) the capacitance for all electrodes has been calculated, and their corresponding values at desired current rates are summarized in Table 1.

$$C = I \times dt / m \times dV, \tag{1}$$

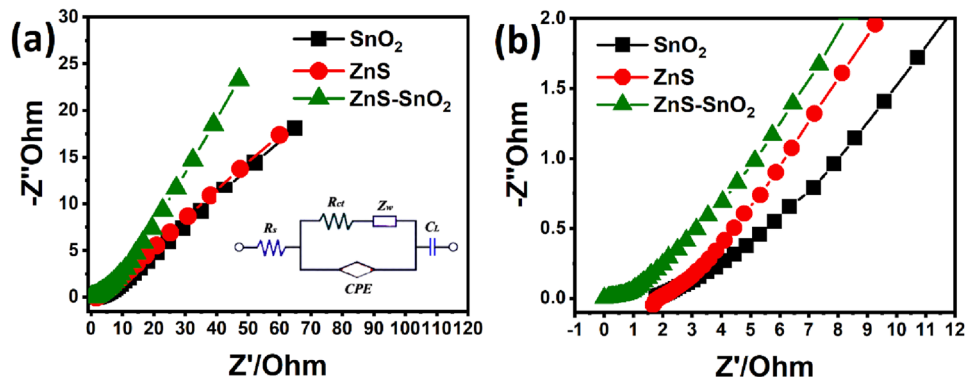
where dt is the discharge time, dV denotes the potential window, and i/m is the discharge current rate.

Table 1 Discharge current and the desired capacitance of the ZnS, SnO₂, and ZnS–SnO₂ composite electrodes

Current density (A g ⁻¹)	ZnS(F/g)	SnO ₂ (F/g)	ZnS–SnO ₂ (F/g)
1	256	172	466
2	216	150	433
3	185	140	375
5	166	125	316
7	140	105	256

The capacitance and current rate graphs are shown in Fig. 5e for a detailed comparison of all electrodes. The graph shows that composting is one of the most effective and scalable techniques, which optimizes

Fig. 6 **a** Impedance plot, inset shows the equivalent circuit model, and **b** zoomed view of the impedance plot of the ZnS, SnO₂, and ZnS–SnO₂ composite electrodes



poor energy storage performance after proper heterostructure formation. In Fig. 5e, we noticed that ZnS is a relatively higher capacitance than SnO₂ due to its high conductivity and vice versa [39]. The high capacitance of the ZnS–SnO₂ composite electrode is due to the synergy between Sn and Zn, which collectively enhanced the charge storage performance in a composite matrix. The honeycomb-like morphology of ZnS offers more active centers and shortens the diffusion of ions during discharge/charge activities, leading to supreme electrochemical properties [53].

The incredible energy storage performance of the ZnS–SnO₂ composite electrode can be assessed using another powerful technique, known as impedance analysis, which indicates the charge transport kinetics, as schematically shown in Fig. 6. The impedance plots for the ZnS, SnO₂, and ZnS–SnO₂ composite electrodes is displayed in Fig. 6a, which showed no semi-circle for all electrodes, manifesting the smallest charge transfer resistance of the electrode materials. All electrodes followed the same trend in their impedance plots. The only variation is that the ZnS–SnO₂ composite electrode exhibits the smallest solution and charge transfer resistances compared with ZnS and SnO₂ electrodes, and the values are tabulated in Table 2. The inset in Fig. 6a depicts the equivalent circuit model, showing resistance, Wurzburg impedance, capacitor, and constant phase element, which perfectly coincide with the impedance analysis. The enlarged view of the impedance plot is shown in Fig. 6b, which supports the above claims. The higher conductivity supports fast kinetics of electrolyte ions, which leads to great rate performance of the host electrode material [54, 55]. According to our earlier results, the smallest charge transfer resistance proved the ZnS higher conductivity. The low conductivity of SnO₂ is the main cause of its poor electrochemical performance.

Table 2 Impedance plot parameters

Sample	ZnS	SnO ₂	ZnS–SnO ₂
Rs	1.62 Ω	1.52 Ω	– 0.03 Ω
Rct	2.15 Ω	2.83 Ω	1.2 Ω

A hybrid supercapacitor was additionally constructed to give a general idea of the optimized ZnS–SnO₂ composite for real-world applications. Herein, we built a ZnS–SnO₂||AC/KOH hybrid supercapacitor with AC and ZnS–SnO₂ composite as the negative and positive electrodes in a conducting medium in KOH as the electrolyte, as schematically shown in Fig. 7a. To perceive the electrochemical energy, storage performance of the ZnS–SnO₂ and AC electrodes were examined in two different potentials to get an optimal voltage for hybrid supercapacitor, as supplemented in Fig. 7b. Based on Fig. 7b, the optimized voltage frame for the as-built ZnS–SnO₂||AC/KOH hybrid supercapacitor was 1.7 V, which seems to be the stable potential. It can be further tested with various scans and current rates. The CV voltammogram at various scans was tested in a voltage limit of 0–1.7 V, which revealed an un-perturbed shape from low to higher scan, demonstrating the high reversibility, excellent power delivery, and rate capability of the ZnS–SnO₂||AC/KOH hybrid supercapacitor (see Fig. 7c). The discharge/charge profile was further measured to check out the chosen voltage is whether stable or not that seems that the 1.7 V voltage cutoff successfully reached to its highest value, indicating the stable voltage of the ZnS–SnO₂||AC/KOH hybrid supercapacitor (Fig. 7d). The pseudocapacitive behavior was confirmed from the non-linearity of the curves at several current rates. It is noticeable that the discharge/charge features sustain their shape till 5 A/g, confirming the pronounced rate performance. The

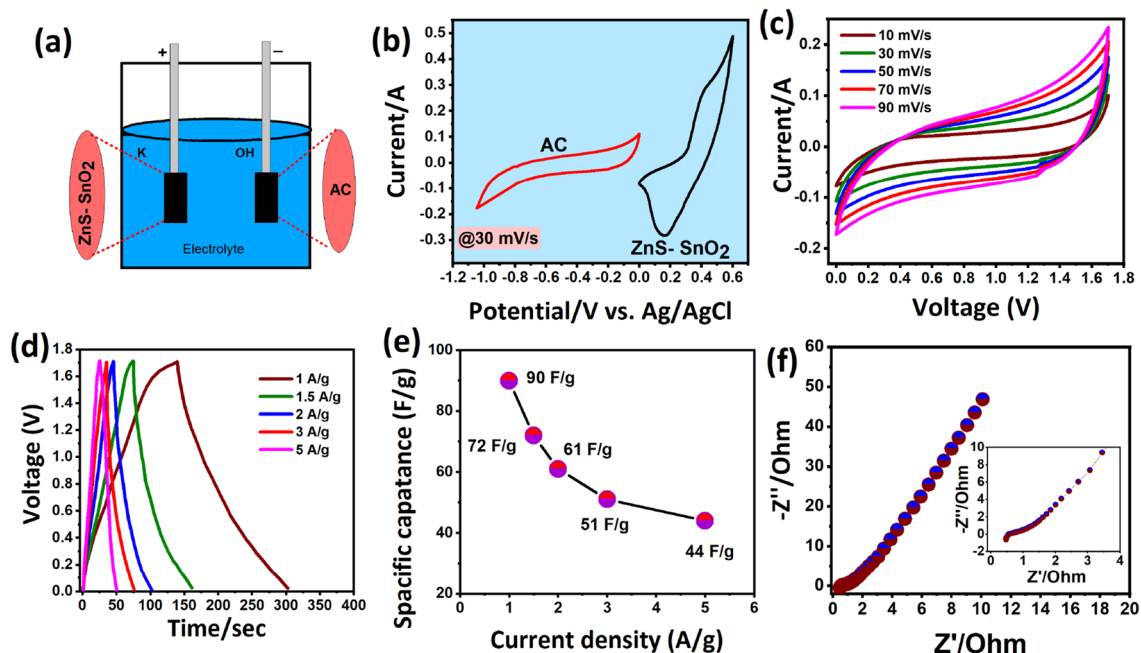


Fig. 7 a schematic of the assembled ZnS–SnO₂//AC/KOH hybrid supercapacitor, b CV curves of AC and ZnS–SnO₂ composite electrodes, c CV curves at various scans, d discharge/charge plot at different current rates, e capacitance plot, f impedance plot

Table 3 Energy, power densities, and capacitance of the ZnS–SnO₂//AC/KOH hybrid supercapacitor

Current density (A/g)	1	1.5	2	3	5
Specific capacitance (F/g)	90	72	61	51	44
Specific energy (Wh/kg)	36.12	28.9	24.5	20.47	17.66
Specific power (W/kg)	855.5	1284.4	1696.2	2541	4238.4

current-dependent capacitance of the ZnS–SnO₂//AC/KOH hybrid supercapacitor was calculated. The results are plotted in Fig. 7e. At the current rates of 1, 1.5, 2, 3, and 5 A/g, a relatively higher capacitance of 90, 72, 61, 51, and 44 F/g was calculated using Eq. (1). These values of the ZnS–SnO₂//AC/KOH hybrid supercapacitor are comparably larger than many previous reports, as ZnO–ZnS–CdS//AC of 140 F/g (1 A/g) [39], ZnS@FeSe₂//AC of 110 F/g (1 A/g) [37], ZnO/SnO₂@NiCo₂O₄@CC//AC@CC (carbon cloth) of 117.5 F/g (0.25 A/g) [56], and ZnS/Ni₃S₂//AC of 127.6 F/g (1 A/g) [57], and the values are also listed in Table 3, respectively. The impedance plot was further measured, which showed a charge transfer resistance of 1.3 ohms and a solution resistance of 0.3 ohms, implying the high conductivity of sufficient electrolyte ions

transmission between the electrode and electrolyte interface, as given in Fig. 7f, an enlarged view in the inset.

The specific energy and power of the ZnS–SnO₂//AC/KOH hybrid supercapacitor are crucial for practical aspects, which can be determined using Eqs. (2 & 3).

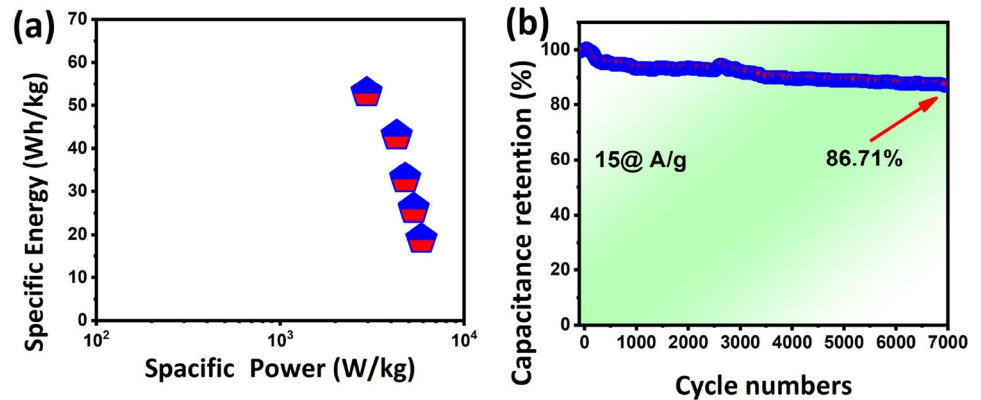
$$E = 1/7.2C \times V^2, \tag{2}$$

$$P = E \times 3600/t. \tag{3}$$

where C, V, and t describe the capacitance, voltage window, and the discharge time difference.

The Ragone plot is given in Fig. 8a. A high-specific energy of 36.12 Wh/kg was obtained, which reached 17.66 Wh/kg when the current rate increased from 1 to 5 A/g. A Maximum power delivery of 4238.4 W/kg was attained, as shown in Fig. 8a; Table 3. The great energy and power delivery were due to the synergy between ZnS and SnO₂, and the high conductivity of the AC supported the superhighway for charge kinetic. The obtained specific power and specific energy of the ZnS–SnO₂//AC/KOH hybrid supercapacitor are higher than the previous reports, such as; ZnS–NiS_{1.97}//AC (25.6 Wh/kg, and 2173.8 W/kg) [58], Fe–SnO₂@CeO₂//AC (32.2 Wh/kg, and 7390

Fig. 8 **a** The specific energy and power delivery plot, **b** stability test of the ZnS–SnO₂||AC/KOH hybrid supercapacitor



W/kg) [59], and Ce–SnO₂@g-C₃N₄//AC (39.3 Wh/kg, and 7425 W/kg) [60], respectively. The stability of the active material is also one of the essential factors to influence the performance of ZnS–SnO₂||AC/KOH hybrid supercapacitor is tested for 7000 cycles at large current rates, as shown in Fig. 8b. A steady and stable durability performance of the ZnS–SnO₂||AC/KOH hybrid supercapacitor was perceived, signifying the good stability of the electrode materials. The steady and stable decay during the cycling test is due to the high conductivity of ZnS and AC that prevented structural collapse and acts as a scaffold during the discharge and charging process.

4 Conclusion

This work portrays the successful and facile sol-gel preparation of ZnS, SnO₂, and ZnS–SnO₂ composite to explore their energy storage performance for hybrid supercapacitors for the first time. The physical characterization, including XRD, Raman analysis, FESEM, and EDX, concluded the adequate synthesis of the samples with high crystallinity and purity without any residues found on their surfaces/phase structures. The CV and discharge/charge measurements confirmed the capacitive signature and pseudocapacitive behavior with prominent redox peaks and noticeable voltage plateaus. The electrochemical investigation showed that the ZnS–SnO₂ composite displayed relatively enhanced electrochemical properties due to its high conductivity and the synergy between ZnS and SnO₂. More specifically, a ZnS–SnO₂||AC/KOH hybrid supercapacitor was further developed, displaying a high capacitance, specific energy Ω , and power delivery, suppressing most existing reports on ZnS-based

other supercapacitors. Thus, our work paves the way to construct other metal oxide-based electrodes for high-power and energy storage domains.

Author contribution

KR: wrote the original paper, designed the experiments, and conducted the whole synthesis work. MZUS, SAA, MA, MSUS: characterize the samples and analyze the data. HH: writing—review and editing. MS: writing—review and editing. AS: co-supervision, writing—review, and editing. NH: writing—review, editing, supervision.

Funding

There is no funding to be declared to support this project.

Data availability

The data related to this study can be available at a reasonable request from the corresponding author.

Declarations

Conflict of interest The author declares no conflict to be declared.

References

1. S.A. Ahmad et al., High power aqueous hybrid asymmetric supercapacitor based on zero-dimensional ZnS nanoparticles with two-dimensional nanoflakes CuSe₂ nanostructures. *Ceram. Int.* **49**(12), 20007–20016 (2023)
2. M. Arif et al., CdS nanoparticles decorated on carbon nanofibers as the first ever utilized as an electrode for advanced energy storage applications. *J. Inorg. Organomet. Polym. Mater.* **33**(4), 969–980 (2023)
3. M.S.U. Shah et al., Nickel selenide nano-cubes anchored on cadmium selenide nanoparticles: first-ever designed as electrode material for advanced hybrid energy storage applications. *J. Energy Storage.* **63**, 107065 (2023)
4. E. Ullah et al., Hydrothermal assisted synthesis of hierarchical SnO₂ micro flowers with CdO nanoparticles based membrane for energy storage applications. *Chemosphere* **321**, 138004 (2023)
5. M. Sajjad et al., Recent trends in transition metal diselenides (XSe₂: X = ni, Mn, Co) and their composites for high energy faradic supercapacitors. *J. Energy Storage* **43**, 103176 (2021)
6. M. Sajjad et al., A review on selection criteria of aqueous electrolytes performance evaluation for advanced asymmetric supercapacitors. *J. Energy Storage.* **40**, 102729 (2021)
7. Ā. Sánchez-Sánchez et al., The importance of electrode characterization to assess the supercapacitor performance of ordered mesoporous carbons. *Microporous Mesoporous Mater.* **235**, 1–8 (2016)
8. V. Velmurugan et al., Synthesis of tin oxide/graphene (SnO₂/G) nanocomposite and its electrochemical properties for supercapacitor applications. *Mater. Res. Bull.* **84**, 145–151 (2016)
9. M.Z.U. Shah et al., A new CuO/TiO₂ nanocomposite: an emerging and high energy efficient electrode material for aqueous asymmetric supercapacitors. *J. Energy Storage* **55**, 105492 (2022)
10. M.Z.U. Shah et al., Copper sulfide nanoparticles on titanium dioxide (TiO₂) nanoflakes: a new hybrid asymmetrical faradaic supercapacitors with high energy density and superior lifespan. *J. Energy Storage* **55**, 105651 (2022)
11. M. Sajjad et al., A novel high-performance all-solid-state asymmetric supercapacitor based on CuSe nanoflakes wrapped on vertically aligned TiO₂ nanoplates nanocomposite synthesized via a wet-chemical method. *J. Energy Storage* **55**, 105304 (2022)
12. B.A. Khan et al., NiSe₂ nanocrystals intercalated rGO sheets as a high-performance asymmetric supercapacitor electrode. *Ceram. Int.* **48**(4), 5509–5517 (2022)
13. J.A. Syed et al., Hierarchical multicomponent electrode with interlaced Ni(OH)₂ nanoflakes wrapped zinc cobalt sulfide nanotube arrays for sustainable high-performance supercapacitors. *Adv. Energy Mater.* **7**(22), 1701228 (2017)
14. C. Zhang et al., All-solid-state asymmetric supercapacitors based on Fe-doped mesoporous Co₃O₄ and three-dimensional reduced graphene oxide electrodes with high energy and power densities. *Nanoscale* **9**(40), 15423–15433 (2017)
15. K. Khan et al., Development of 1.6 V hybrid supercapacitor based on ZnO nanorods/MnO₂ nanowires for next-generation electrochemical energy storage. *J. Electroanal. Chem.* **922**, 116753 (2022)
16. M.Z.U. Shah et al., A novel TiO₂/CuSe based nanocomposite for high-voltage asymmetric supercapacitors. *J. Science: Adv. Mater. Devices* **7**(2), 100418 (2022)
17. M.Z.U. Shah et al., Hydrothermal synthesis of ZnO@ ZnS heterostructure on ni foam: a binder free electrode for high power and stable hybrid supercapacitors. *Mater. Lett.* **326**, 132910 (2022)
18. M. Sajjad, W. Lu, Covalent organic frameworks based nanomaterials: design, synthesis, and current status for supercapacitor applications: a review. *J. Energy Storage.* **39**, 102618 (2021)
19. M. Sajjad, W. Lu, Honeycomb-based heterostructures: an emerging platform for advanced energy applications: a review on energy systems. *Electrochem. Sci. Adv.* **2**(5), e202100075 (2022)
20. J. Li et al., Three-dimensional nitrogen and phosphorus co-doped carbon quantum dots/reduced graphene oxide composite aerogels with a hierarchical porous structure as superior electrode materials for supercapacitors. *J. Mater. Chem. A* **7**(46), 26311–26325 (2019)
21. K. Chen et al., Structural design of graphene for use in electrochemical energy storage devices. *Chem. Soc. Rev.* **44**(17), 6230–6257 (2015)
22. J. Ismail et al., Comparative capacitive performance of MnSe encapsulated GO based nanocomposites for advanced electrochemical capacitor with rapid charge transport channels. *Mater. Chem. Phys.* **284**, 126059 (2022)
23. M. Sajjad et al., A new CuSe–TiO₂–GO ternary nanocomposite: realizing a high capacitance and voltage for an advanced hybrid supercapacitor. *Nanomaterials* **13**(1), 123 (2022)
24. Z. Yang et al., Vertically-aligned Mn(OH)₂ nanosheet films for flexible all-solid-state electrochemical supercapacitors. *J. Mater. Sci. Mater. Electron.* **28**(23), 17533–17540 (2017)
25. X. Jia, X. Wu, B.J.D.T. Liu, Formation of ZnCo₂O₄@ MnO₂ core–shell electrode materials for hybrid supercapacitor. *Dalton Trans.* **47**(43), 15506–15511 (2018)

26. H. Liu et al., Boosting energy storage and electrocatalytic performances by synergizing $\text{CoMoO}_4@ \text{MoZn}_{22}$ core-shell structures. *Chem. Eng. J.* **373**, 485–492 (2019)
27. K. Tao et al., A metal–organic framework derived hierarchical nickel–cobalt sulfide nanosheet array on Ni foam with enhanced electrochemical performance for supercapacitors. *Dalton Trans.* **47**(10), 3496–3502 (2018)
28. X. Han et al., Design of a porous cobalt sulfide nanosheet array on Ni foam from zeolitic imidazolate frameworks as an advanced electrode for supercapacitors. *Nanoscale* **10**(6), 2735–2741 (2018)
29. G. Yuan et al., $\text{Cu/Cu}_2\text{O}$ nanostructures derived from copper oxalate as high performance electrocatalyst for glucose oxidation. *Chin. Chem. Lett.* **31**(7), 1941–1945 (2020)
30. T.N. Trindade, L.A.J.J.o.A., Silva, Compounds, Cd-doped SnO_2/CdS heterostructures for efficient application in photocatalytic reforming of glycerol to produce hydrogen under visible light irradiation. *J. Alloys Compd.* **735**, 400–408 (2018)
31. N. Bhardwaj, S.J.C.I. Mohapatra, Structural, optical and gas sensing properties of Ag-SnO_2 plasmonic nanocomposite thin films. *Ceram. Int.* **42**(15), 17237–17242 (2016)
32. S. Ren et al., Hollow SnO_2 microspheres and their carbon-coated composites for supercapacitors. *Colloids Surf. A: Physicochem. Eng. Asp.* **444**, 26–32 (2014)
33. L. Yu et al., Hydrothermal synthesis of SnO_2 and $\text{SnO}_2@ \text{C}$ nanorods and their application as anode materials in lithium-ion batteries. *RSC Adv.* **3**(38), 17281–17286 (2013)
34. B. Saravanakumar et al., Enhanced pseudocapacitive performance of SnO_2 , ZnS-SnO_2 , and Ag-SnO_2 nanoparticles. *Ionics* **24**(12), 4081–4092 (2018)
35. H. Chen et al., Highly conductive $\text{NiCo}_2 \text{S}_4$ urchin-like nanostructures for high-rate pseudocapacitors. *Nanoscale* **5**(19), 8879–8883 (2013)
36. Y. Gao et al., Double metal ions synergistic effect in hierarchical multiple sulfide microflowers for enhanced supercapacitor performance. *ACS Appl. Mater. Interfaces* **7**(7), 4311–4319 (2015)
37. S.A. Ahmad et al., Facile synthesis of hierarchical $\text{ZnS}@ \text{FeSe}_2$ nanostructures as new energy-efficient cathode material for advanced asymmetric supercapacitors. *J. Science: Adv. Mater. Devices* **7**(4), 100489 (2022)
38. K. Krishnamoorthy et al., One pot hydrothermal growth of hierarchical nanostructured Ni_3S_2 on Ni foam for supercapacitor application. *Chem. Eng. J.* **251**, 116–122 (2014)
39. S. BiBi et al., A new ZnO-ZnS-CdS heterostructure on Ni substrate: a binder-free electrode for advanced asymmetric supercapacitors with improved performance. *Electrochim. Acta* **430**, 141031 (2022)
40. N.S. Arul, L. Cavalcante, J. In Han, Facile synthesis of ZnS/MnS nanocomposites for supercapacitor applications. *J. Solid State Electrochem.* **22**(1), 303–313 (2018)
41. R. Ramachandran et al., Solvothermal synthesis of zinc sulfide decorated graphene (ZnS/G) nanocomposites for novel supercapacitor electrodes. *Electrochim. Acta* **178**, 647–657 (2015)
42. X. Hou et al., Ultrathin ZnS nanosheet/carbon nanotube hybrid electrode for high-performance flexible all-solid-state supercapacitor. *Nano Res.* **10**(8), 2570–2583 (2017)
43. K. Patel, M. Deshpande, S. Chaki, Doping-induced changes in the structural, optical, magnetic and thermal properties of Ni: ZnS nanoparticles prepared by microwave-assisted chemical method. *Appl. Phys. A* **127**(10), 1–8 (2021)
44. U. Gawai, B. Dole, Local structural studies on Co doped ZnS nanowires by synchrotron X-ray atomic pair distribution function and micro-Raman shift. *RSC Adv.* **7**(59), 37402–37411 (2017)
45. R. Katiyar et al., Dynamics of the rutile structure. III. Lattice dynamics, infrared and Raman spectra of SnO_2 . *J. Phys. C: Solid State Phys.* **4**(15), 2421 (1971)
46. K. Yu et al., Microstructural change of nano- SnO_2 grain assemblages with the annealing temperature. *Phys. Rev. B* **55**(4), 2666 (1997)
47. M. Sajjad et al., Low-temperature synthesis of 3D copper selenide micro-flowers for high-performance supercapacitors. *Mater. Lett.* **314**, 131857 (2022)
48. M. Sajjad et al., CuCo_2O_4 nanoparticles wrapped in a rGO aerogel composite as an anode for a fast and stable Li-ion capacitor with ultra-high specific energy. *New J. Chem.* **45**(44), 20751–20764 (2021)
49. M. Sajjad, Y. Khan, Rational design of self-supported Ni_3S_2 nanoparticles as a battery type electrode material for high-voltage (1.8 V) symmetric supercapacitor applications. *CrystEngComm* **23**(15), 2869–2879 (2021)
50. M. Sajjad, R. Tao, L. Qiu, Phosphine based covalent organic framework as an advanced electrode material for electrochemical energy storage. *J. Mater. Sci.: Mater. Electron.* **32**(2), 1602–1615 (2021)
51. M. Sajjad et al., Phosphine-based porous organic polymer/rGO aerogel composites for high-performance asymmetric supercapacitor. *ACS Appl. Energy Mater.* **4**(1), 828–838 (2021)
52. M. Sajjad et al., Bismuth Yttrium Oxide (Bi_3YO_6), a new electrode material for asymmetric aqueous supercapacitors. *J. Inorg. Organomet. Polym. Mater.* **31**(3), 1260–1270 (2021)
53. A. Ali et al., Honeycomb like architectures of the Mo doped $\text{ZnS}@ \text{Ni}$ for high-performance asymmetric

- supercapacitors applications. *Synth. Met.* **265**, 116408 (2020)
54. M. Sajjad, Y. Khan, W. Lu, One-pot synthesis of 2D SnS₂ nanorods with high energy density and long term stability for high-performance hybrid supercapacitor. *J. Energy Storage* **35**, 102336 (2021)
55. X. Zhao et al., Covalent organic framework templated ordered nanoporous C60 as stable energy efficient supercapacitor electrode material. *Carbon*. **182**, 144–154 (2021)
56. N. Kitchamsetti, D. Kim, Facile synthesis of hierarchical core–shell heterostructured ZnO/SnO₂@ NiCo₂O₄ nanorod sheet arrays on carbon cloth for high performance quasi-solid-state asymmetric supercapacitors. *J. Mater. Res. Technol.* **21**, 590–603 (2022)
57. X. Li et al., Cactus-like ZnS/Ni₃S₂ hybrid with high electrochemical performance for supercapacitors. *J. Alloys Compd.* **753**, 508–516 (2018)
58. C. Wei et al., Self-template synthesis of double shelled ZnSN–iS₁. 97 hollow spheres for electrochemical energy storage. *Appl. Surf. Sci.* **435**, 993–1001 (2018)
59. S. Asaithambi et al., Preparation of Fe–SnO₂@ CeO₂ nanocomposite electrode for asymmetric supercapacitor device performance analysis. *J. Energy Storage* **36**, 102402 (2021)
60. S. Asaithambi et al., The bifunctional performance analysis of synthesized ce doped SnO₂/g-C₃N₄ composites for asymmetric supercapacitor and visible light photocatalytic applications. *J. Alloys Compd.* **866**, 158807 (2021)

Publisher's Note Springer Nature remains neutral with regard to jurisdictional claims in published maps and institutional affiliations.

Springer Nature or its licensor (e.g. a society or other partner) holds exclusive rights to this article under a publishing agreement with the author(s) or other rightsholder(s); author self-archiving of the accepted manuscript version of this article is solely governed by the terms of such publishing agreement and applicable law.